ODAS 2016 Full Paper

TITLE: Multi-sensor **s**atellite-based monitoring of a volcanic eruption
NAME & First name of main author: PLANK, Simon
Address (Department/Institute): German Aerospace Center (DLR), German Remote Sensing Data Center (DFD), Geo-Risks and Civil Security (GZS)
E-mail address of main author: simon.plank@dlr.de
Phone number of main author: +49 8153 28 3460
Date of birth of all authors: 07 March 1984

Abstract

This paper presents a combined analysis of multi-sensor satellite-based remote sensing data monitoring of a volcanic eruption – the 2014/15 Holuhraun fissure eruption in Iceland. Signalized by increasing seismic activity on 16 August 2014 onwards, a dike originated from the Bardarbunga Volcano broke through the Earth's surface on 29 August 2014, causing one of the largest volcanic events in modern Icelandic history. Within this multi-sensor approach three different aspects are investigated: First, the development of the hotspot was monitored by analyzing MODIS imagery and satellite data of DLR's FireBIRD mission (TET-1 – Technology Experiment Carrier).
Second, gases emitted by the volcano, such as SO_2 were investigated using data from satellites focusing on atmospheric remote sensing. SO_2 total columns are retrieved from the ultraviolet spectrometer GOME-2 onboard the polar satellites MetOp-A and -B. Earthshine reflectances from nadir-view scans are measured by GOME-2 on a daily basis. SO_2 emissions showed a strong increase when the fissure first erupted in late August 2014.
Comparison with higher spatial resolution Earth observation satellite imagery showed a strong correlation between the development of the area covered by lava and the amount of SO_2 emitted by the volcano. A time series of synthetic aperture radar (SAR) imagery acquired by TerraSAR-X and Sentinel-1 as well as a dataset of ASTER and Landsat-8 daytime and nighttime and WorldView-2/-3 acquisitions was used to monitor the spatio-temporal evolution of the lava extent.

1. Introduction

The Holuhraun fissure eruption in 2014/15, a dike intrusion originating from the Bardarbunga Volcano, is one of the largest eruptions in modern Icelandic history. The Bardarbunga system is located in the Eastern Volcanic Zone and extends to a length of 190 km and width of 25 km [1]. The central volcano of Bardarbunga which is partly covered by the Vatnajökull icecap [2] consists of a central volcano rising to an elevation of 2009 m above sea level and a fissure swarm. The swarm is characterized by explicit tensional tectonics. Bardarbunga volcano is subject to extensive seismic monitoring and GPS networks by the Icelandic Meteorological Office [1].

The 2014/15 event was a subaerial fissure eruption but several minor subglacial eruptions may have also appeared in the two weeks prior to the main event. Preceding signals including seismic activity steadily developed over a period of seven years in both the caldera and the northward extending fissure swarm. Although the activity partially decreased after the May

2011 Grímsvötn eruption, it soon inclined to peak two weeks before the eruption. GPS networks furthermore noticed ground deformation [1]. The first clearly detectable eruption established on 29 August 2014 around 4.5 km from the ice margin of Dyngjujokull glacier. By the end of its active period on 28 February 2015 the lava field covered an area of 85 km². The total volume measured 1.4 km³ [3].

This study aims to investigate the temporal evolution of the Holuhraun fissure eruption by means of multi-sensor remote sensing. Section 2 gives a short summary of the development of the volcanic eruption. Section 3.1 focuses on thermal hotspot detection using data from MODIS and TET. Section 3.2 presents the analysis of volcanic gas eruptions measured by atmospheric remote sensing. The spatio-temporal evolution of the lava extent is investigated in section 3.3 by means of synthetic aperture radar (SAR) and multispectral remote sensing sensors. Finally, section 4 presents a combined analysis of the results presented in sections 3.1 to 3.3.

2. Development of the eruption

Increasing seismic activity from 16 August 2014 onwards, starting at the caldera but subsequently migrating, signalized the development of a dike. Seismic tremor on 23 August indicated a lava eruption beneath Dyngjujokull glacier which enlarged over the following days. The eruption was first documented at the surface about 45 km north-east of the caldera on 29 August when reaching the outboard of the Vatnajokull ice cap while venting along a mature fissure [3]. The eruption was effusive and moderate [4]. On 31 August lava erupted along a 1.5 km long fissure.

Observations in early September verified a white steam-and-gas plume rising to 4.5 km and drifting, lava flowing and lava fountains to heights of tens of meters, high gas emissions and elevated seismicity. Ash production was almost negligible. As the eruption continued, on 5 September two new but less effusive eruptive figures appeared. During September gas emissions, including SO_2, and lava continued at consistent rates and partly interacted with the Jökulsá á Fjöllum river producing steam but no explosive activity. The first 1.5 months of the eruption created an average flux of SO_2 of 400 kg/s (~35,000 metric tons per day, t/d) with peaks reaching up to 1300 kg/s.

Analysis performed from 17 to 23 September demonstrated that the source of the magma lies at a depth exceeding 10 km and 90% of the SO_2 emerged at the active craters. Induced by restrictions to low levels, plumes affected air quality locally in Iceland. While the lava extent expanded significantly especially in the beginning of the eruption the development eased out reaching late December. By the end of September the extent reached 46 km^2.

In October seismicity generally declined despite continuous lava field growth to 65.7 km^2 by the end of the month and 75 km^2 by 30 November. Although eruption intensity decreases in early December, the very gas-rich emissions affected entire Iceland. In late December lava thicknesses were measured to be around 10 m in the eastern part, 12 m in the center and at least 14 m in the western part. During January the lava field kept expanding along its northern and north-eastern margins accompanied by local air pollution. By mid-January 2015 the fissure has extended to a length of over 18 km while covering an area of approximately 84 km² by lava. In late January the lava field thickened instead of further spreading, reaching total volumes of ca. 1.4 km^3.

February is characterized by decreasing eruptive activity and by 17-19 February only one vent remained active inside the crater. The eruption ceased on 28 February 2015 ultimately covering an area of 85 km³. Field studies performed in early March showed no signs of activity [3].

3. Analysis of satellite data

3.1. Thermal hotspot detection

First, the development of the hotspot was monitored by analyzing MODIS imagery and satellite data of DLR's FireBIRD mission (TET-1, Technology Experiment Carrier). MODIS (Moderate Resolution Imaging Spectrometer) flies on NASA's Terra and Aqua satellites with 4 overpasses per day. The NASA fire product MOD14A1 derived from the 1 km spatial resolution MODIS imagery using the 3.9 µm and 11 µm bands is used for hotspot detection. A time series analysis of the MODIS fire product was executed. Fig. 1 shows two examples of the detected hotspot. The volcanic eruption is clearly visible in this low spatial resolution dataset. Comparison of the acquisition of 31 August 2014, which was acquired shortly after the beginning of the eruption, with the one acquired on 17 October 2014 shows an increase of the "fire" area. This increase of the hot area matches very well with the spatio-temporal evolution of the lava extent derived from higher spatial resolution optical and SAR sensors (cf. section 3.3).

TET was launched in 2012 and provides data of ca. 178 m spatial resolution. The mid-wave infrared channel of TET is ideal for the detection of high temperature events. Fig. 2 shows as an example a thermal imagery of TET acquired on 20 September 2014. The cold area of the Vatnajökull Glacier is clearly visible as a dark object in the middle of the scene. South of the glacier the sander, transporting melting water from glacier to the ocean, is visible. The area south-east of the glacier is covered by clouds. North-east of the glacier, the detected hotspot signature marks the location of the fissure eruption.

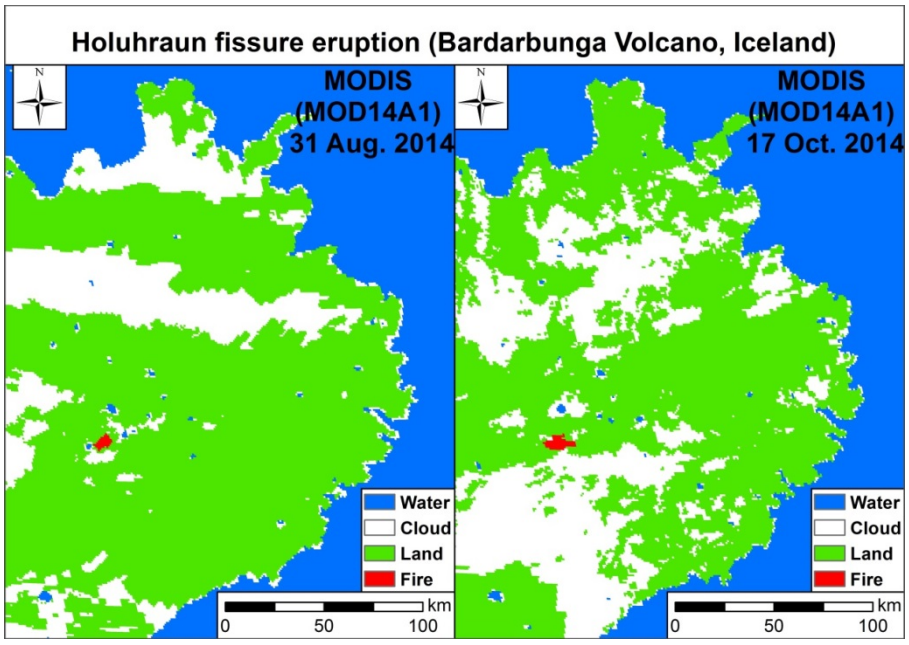

Fig. 1: The Holuhraun fissure eruption monitored by MODIS. Results of the MOD14A1 fire product for 31 August 2014 and 17 October 2014. © NASA 2014.

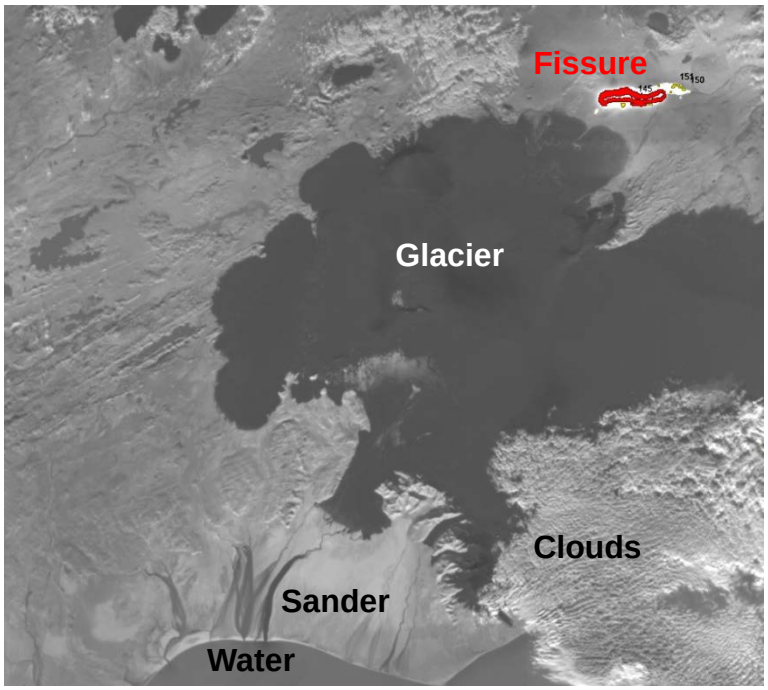

Fig. 2: TET image of the Holuhraun fissure eruption: dark (cold): glacier; red: detected hotspot: fissure eruption. © DLR 2014.

3.2. SO_2 Measurements using GOME-2

High densities of atmospheric SO_2 are an indicator of either anthropogenic pollution or volcanic eruptions. The lifetime of SO_2 ranges from a few days in the troposphere to several weeks in the stratosphere. Ground-based measurements provide high temporal resolution. However, such measurements can only be applied locally. Contrary to this, satellite-based measurements enable a global coverage with the disadvantage of a lower temporal resolution. Satellite-based measurements are well suited for detection of SO_2 anomalies, which might be an indicator for a volcanic eruption.

The emission of volcanic gases due to the 2014/15 Holuhraun fissure eruption was investigated by SO_2 measurements derived from GOME-2 data. The data was kindly provided by Dr. Pascal Hedelt (Remote Sensing Technology Institute (IMF), DLR). The processing of GOME-2 SO_2 data is based on the differential optical absorption spectroscopy (DOAS) method in the UV wavelength range around 320 nm [5-8]. GOME-2 is an ultraviolet spectrometer (290-790 nm) aboard the polar-orbiting satellites MetOp-A (launched in 2006) and MetOp-B (launched in 2012) which takes global measurements of atmospheric composition on a daily basis. GOME-2 provides nadir-view scans with a ground pixel resolution of 40 x 40 km^2 (MetOp-A) and 80 x 40 km^2 (MetOp-B).

To investigate the temporal evolution of the SO_2 emission during the Holuhraun fissure eruption a time series analysis of the SO_2 measurements was executed. The Fig. 3 shows monthly averages for a 50 km radius around the fissure eruption. The data lack between mid of October 2014 and mid of February 2015 is due to the artic night during winter. As Iceland is located at high latitudes, there is no solar radiation during winter. Being a passive sensor, GOME-2 depends on solar radiation. Therefore, no SO_2 measurements are possible during the artic night. The measurements clearly show an increase of the SO_2 emission in late August 2014 when the fissure eruption began. After the data lack during the artic night one can rec-

ognize a decrease of the atmospheric SO_2 total column density. After the end of the volcanic eruption in the end of February 2015 the average SO_2 density is more or less at the same low level as for the beginning of the volcanic eruption.

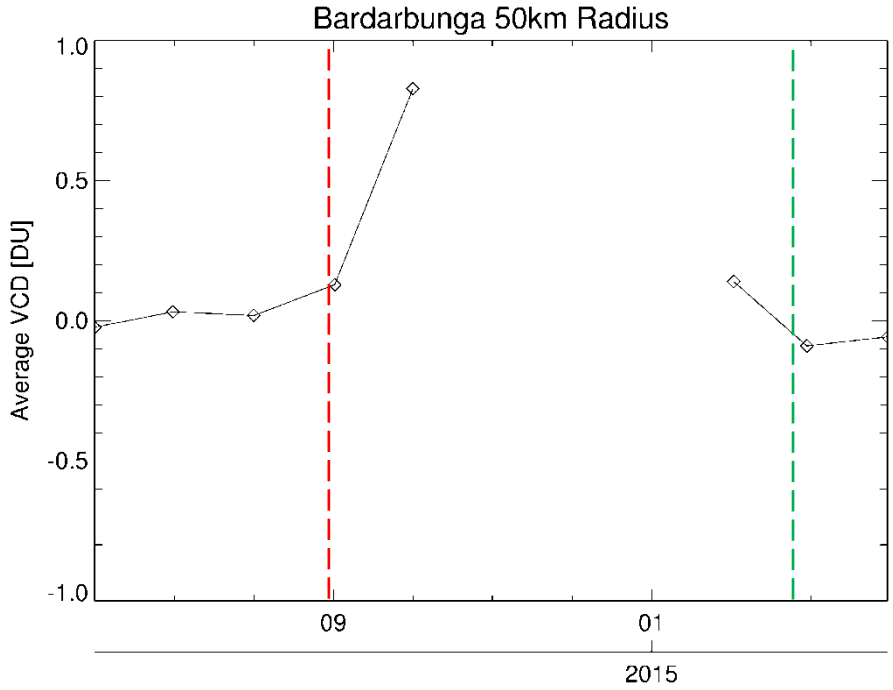

Fig. 3: Monthly average of the SO_2 measurements; 50 km radius around the volcano. The red line marks the beginning of the fissure eruption on 29 August 2014. The green line its end on 28 February 2015.

3.3. Evolution of the lava coverage monitored by SAR and optical imagery

To monitor the spatio-temporal evolution of the lava extent a time series of SAR and optical imagery was used (see Tab.1). The Advanced Spaceborne Thermal Emission and Reflection Radiometer (ASTER) is an advanced multispectral imager that was launched on board NASA's Terra spacecraft in December, 1999. ASTER covers a wide spectral region with 14 bands from the visible to the thermal infrared with high spatial, spectral and radiometric resolution: 15 m in the visible and near-infrared (NIR), 30 m in the short wave infrared (SWIR) and 90 m in the thermal infrared (TIR). Landsat-8, launched on 11 February 2013 by NASA and operated by the United States Geological Survey (USGS) provides imagery at high spatial resolution of 15 m for the panchromatic, 30 m for the multispectral (MS) and 100 m for the TIR bands. The MS bands operate in the visible, NIR and SWIR.

Fig. 4 shows a false color Landsat-8 image of the area of interest one day before the volcanic dike broke through the Earth's surface. For comparison, a very early state of the Holuhraun fissure eruption is shown in Fig. 5. The R/G/B band combination used in these two Landsat-8 images is 7/5/3, i.e. SWIR/NIR/GREEN. The hottest liquid lava parts have a high signature in the NIR channel (green). The outer parts of the lava already cooled down to a solid surface and show a high signature at the longer SWIR band (red). As explained by the Wien's Displacement Law, when the temperature of a blackbody radiator increases, the overall radiated energy increases and the peak of the radiation curve moves to shorter wavelengths. Therefore, the hottest liquid parts of the fissure have a higher signal in the shorter NIR than in the longer SWIR channel.

The TIR channel of Landsat-8 is very suited for nighttime acquisitions of volcanic eruptions. Due to missing solar irradiation, only the thermal emission of the hot lava field is measured. Figure 6 shows a nighttime Landsat-8 imagery acquired on 24 October 2014 over the Holuhraun fissure eruption. The shape of the entire lava field is visible. The hottest parts of the lava are very dominant in this figure. Comparison of the Figs. 5 and 6 shows a change of the location of the fissure, i.e. the location where the liquid lava is erupted.

Tab. 1: Earth observation satellite data used in this study

Satellite	**Dates**				
MODIS [MS, thermal]	Daily: 28/08/2014 to 02/04/2015				
TET-1 [MS]	10/09/2014	14/09/2014	15/09/2014	20/09/2014	23/09/2014
TerraSAR-X [SAR]	30/08/2014 04/09/2014 05/09/2014	15/09/2014 20/09/2014	07/10/2014 18/10/2014	29/10/2014 14/11/2014	19/11/2014 01/12/2014
Sentinel-1 [SAR]	06/10/2014 08/10/2014 13/10/2014 18/10/2014 23/10/2014 25/10/2014 27/10/2014 30/10/2014	06/11/2014 11/11/2014 20/11/2014 23/11/2014 05/12/2014 12/12/2014 24/12/2014 27/12/2014	29/12/2014 05/01/2015 07/01/2015 10/01/2015 15/01/2015 17/01/2015 22/01/2015 29/01/2015	31/01/2015 03/02/2015 05/02/2015 10/02/2015 12/02/2015 15/02/2015 17/02/2015 22/02/2015	27/02/2015 01/03/2015 06/03/2015 11/03/2015 13/03/2015
Landsat-8 [MS, thermal]	28/08/2014 06/09/2014 22/09/2014	29/09/2014 08/10/2014 15/10/2014	24/10/2014 09/11/2014 16/11/2014	18/11/2014 27/12/2014 03/01/2015	05/01/2015 04/02/2015 02/04/2015
ASTER [MS, thermal]	16/09/2014 23/09/2014 28/09/2014	30/10/2014 08/11/2014 10/11/2014	24/11/2014 12/12/2014 17/12/2014	28/12/2014 02/01/2015 11/01/2015	13/01/2015 05/02/2015
WorldView-2 [MS]	29/10/2014				
WorldView-3 [MS]	07/11/2014				

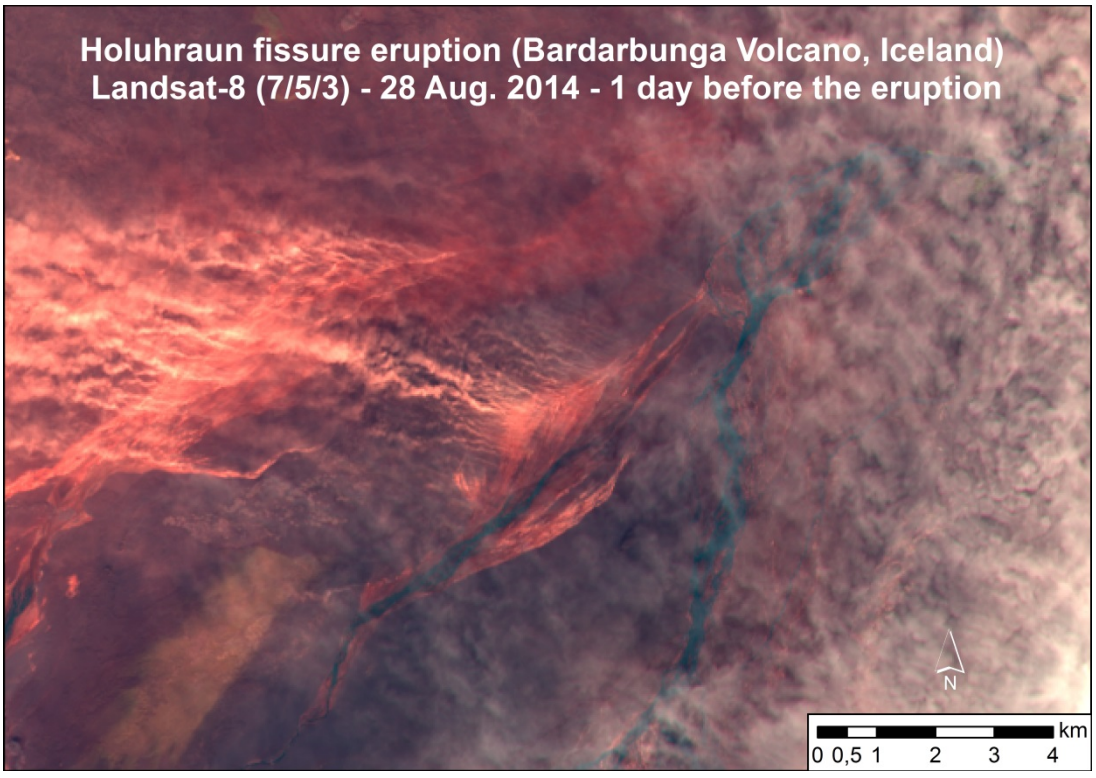

Fig. 4: Area of the Holuhraun fissure eruption one day before the eruption. Landsat-8 © USGS 2014.

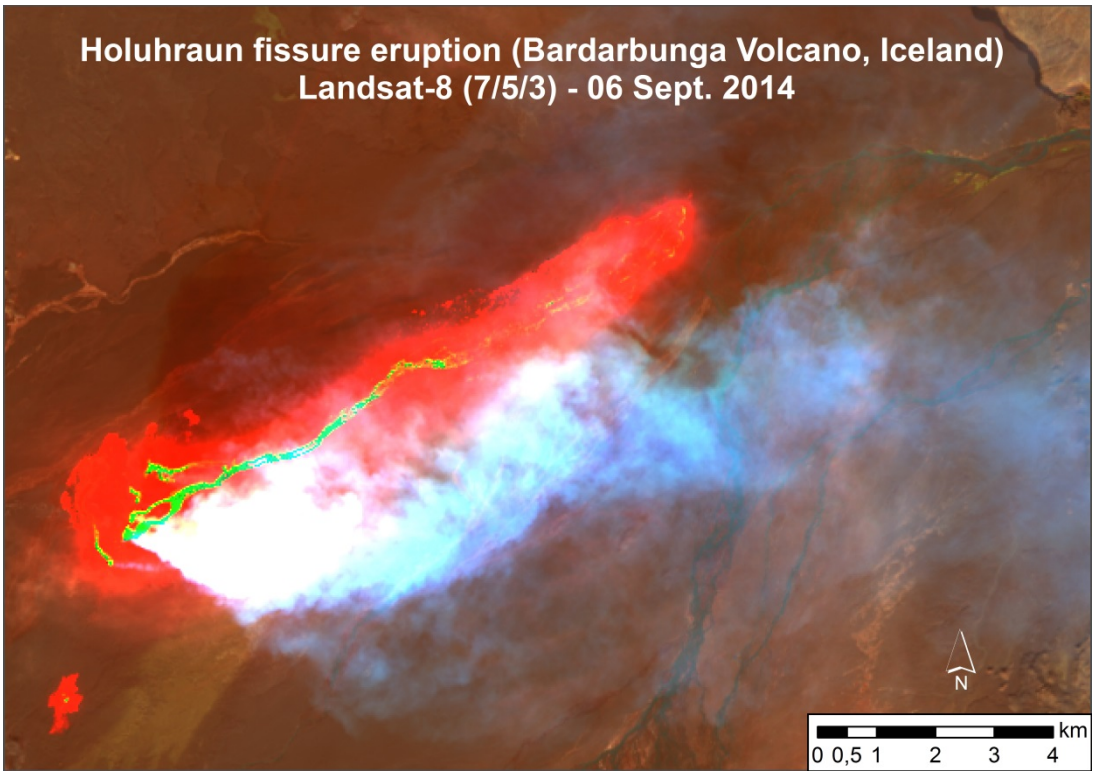

Fig. 5: False color Landsat-8 image of the Holuhraun fissure eruption at a very early state (6 September 2014). Landsat-8 © USGS 2014.

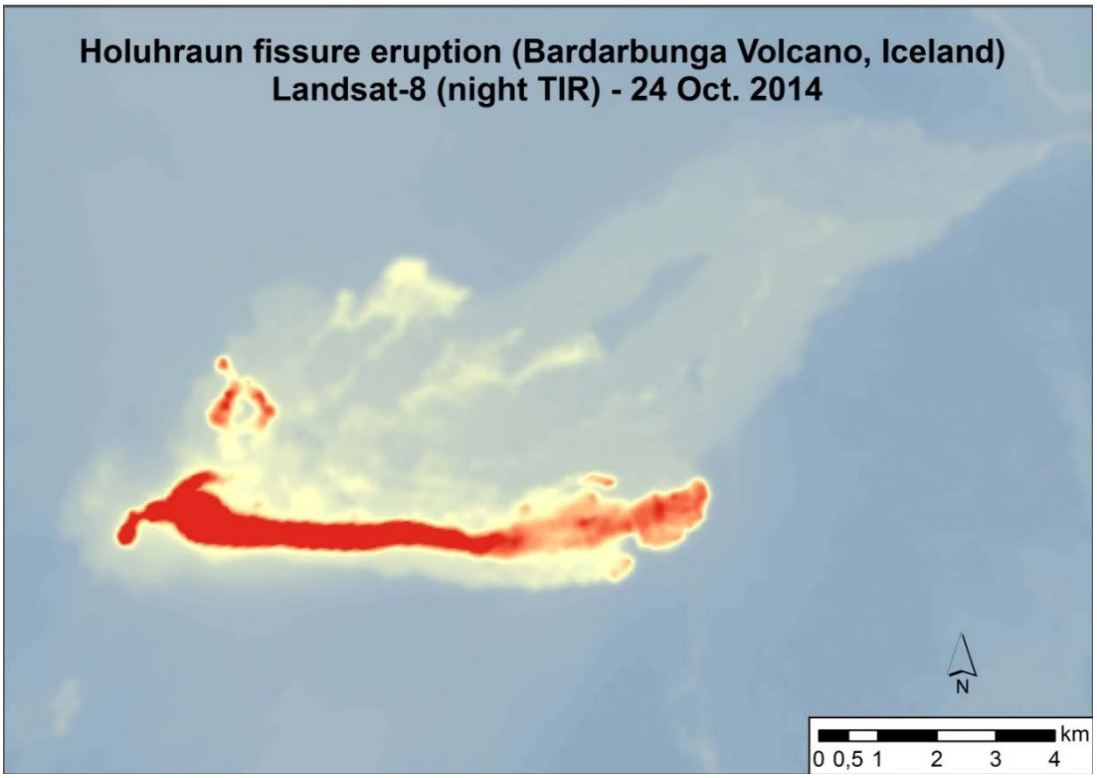

Fig. 6: Nighttime thermal infrared Landsat-8 image of the Holuhraun fissure eruption (24 October 2014). Landsat-8 © USGS 2014.

As SAR is an active sensor, it is independent of the solar radiation and provides useful imagery at day and night. Therefore, also during the arctic night, SAR imagery provides infor-

mation about the spatio-temporal evolution of the fissure eruption and the lava extent. Moreover, due to its longer wavelength compared to optical sensors, SAR is almost complete weather independent and even able to look through volcanic ash plumes.

In this article a series of Sentinel-1 and TerraSAR-X SAR imagery was analyzed. Sentinel-1 was launched on 3 April 2014 by the European Space Agency (ESA). It provides with its C-band SAR antenna imagery with 5 m x 20 m spatial resolution (with the standard interferometric wide swath mode) [9]. The German TerraSAR-X sensor, launched on 15 June 2007 operates in the shorter X-band and provides higher spatial resolution imagery (up to 1 m).

The Figs. 7 and 8 show two examples of a TerraSAR-X and a Sentinel-1 image of the Holuhraun fissure eruption acquired on 1 December 2014 and 17 January 2015, respectively. The Shannon entropy derived from dual-pol TerraSAR-X imagery is a measure of the surface's roughness [10]. The new fresh lava is clearly distinguishable from its surroundings. The new lava is characterized by a higher roughness compared to the surrounding older lava fields, which have a smoother surface due to weathering processes and which are in a large part covered by snow showing a lower roughness (cf. also Fig. 12).

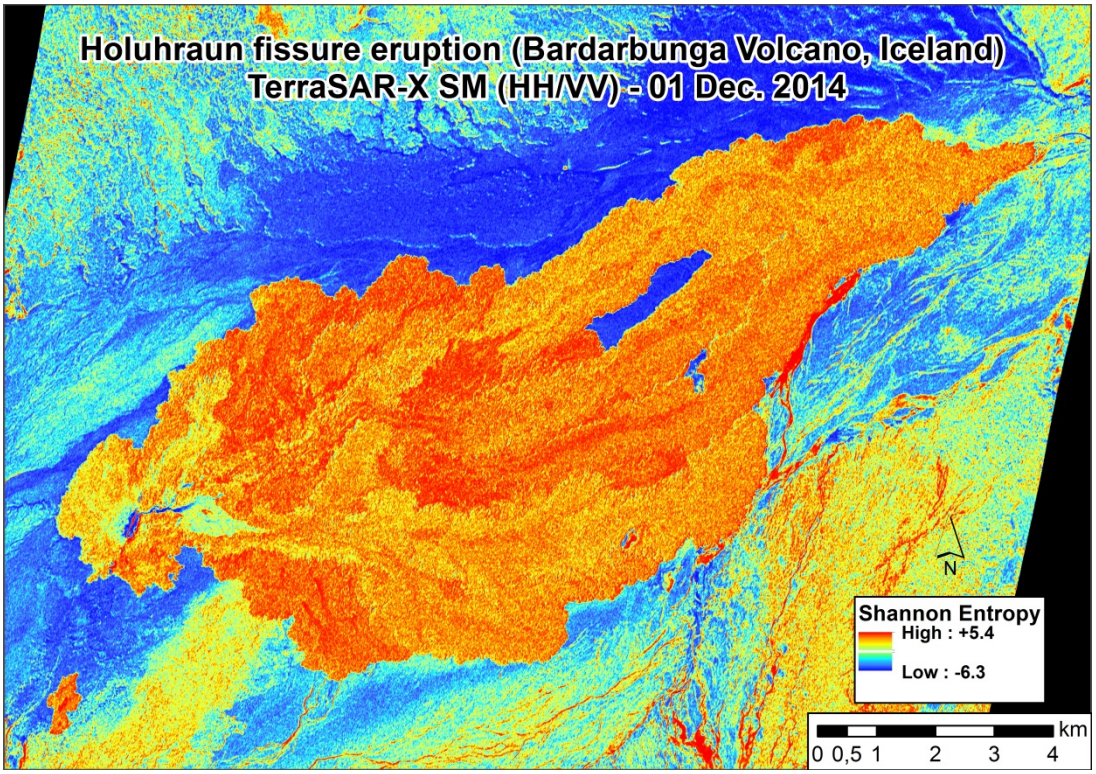

Fig. 7: Shannon entropy derived from dual-pol TerraSAR-X imagery acquired over the Holuhraun fissure eruption on 1 December 2014. TerraSAR-X © 2014 German Aerospace Center (DLR), 2014 Airbus Defence and Space/Infoterra GmbH.

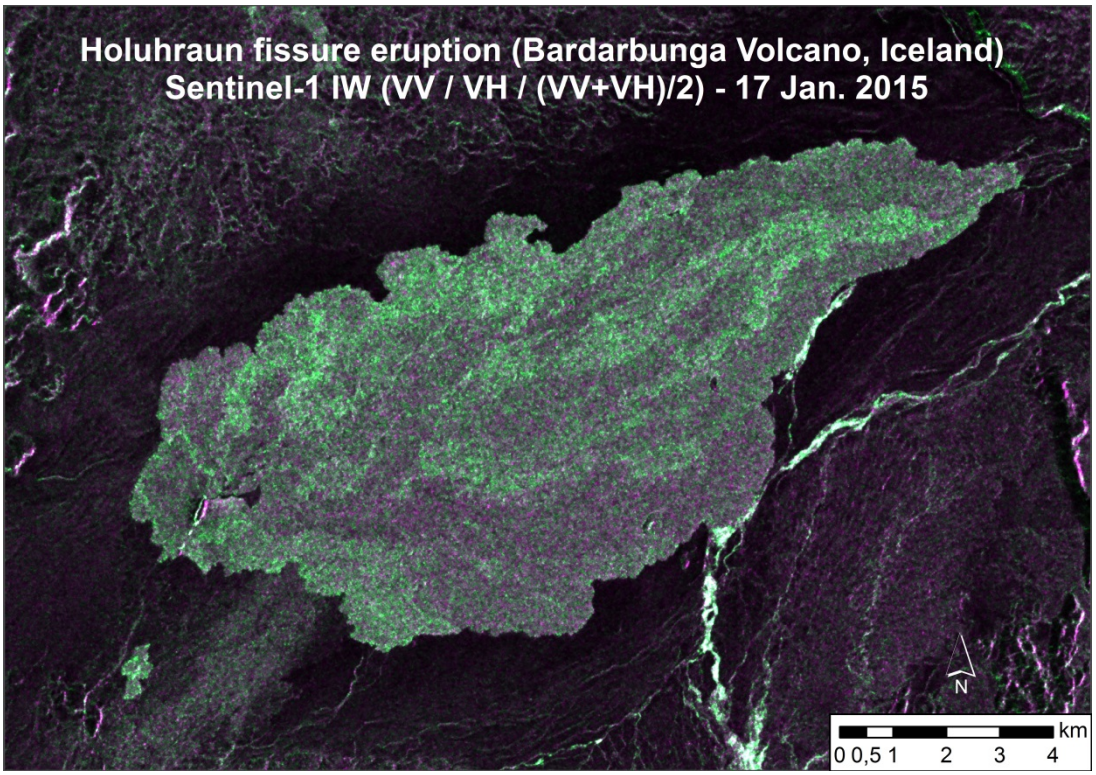

Fig. 8: Dual-pol RGB composite of a Sentinel-1 acquisition over the Holuhraun fissure eruption (17 January 2015). Copernicus Sentinel data [2015].

To support the interpretation of the satellite images, two field photographs of the Icelandic Krafla lava field are shown in Fig. 9. The Krafla volcano, located ca. 90 km north of the Holuhraun fissure eruption, erupted in 1984. Both eruptions, the one of the Krafla volcano and the Holuhraun fissure eruption, produced basaltic lava. One can clearly see the different surface roughness of lava and snow (Fig. 9 left) and of young and old lava (Fig. 9 right).

The Figs. 10 and 11 show the spatio-temporal evolution of the lava extent at the Holuhraun fissure eruption. The measurements are based on visual analysis and manual digitization of the time series of TerraSAR-X and Sentinel-1 SAR imagery. In addition, a time series of cloud-free optical imagery of Landsat-8 and ASTER were analyzed and used to fill gaps in the time series. Moreover, two high spatial resolution WorldView-2 and -3 images with resolutions up to 0.31 m were used for validation and detailed analysis of the area covered by lava (cf. Tab. 1 and Fig. 12).

The measurements show a strong increase of the lava coverage over time. The area covered by lava continuously increased till the end of December 2014. However, the strongest increase of the lava field was during the first months of the eruption. The intensity of lava accumulation decreased over time. By the end of the volcanic eruption on 28 February 2015, the fissure has extended to a length of over 18 km. An area of approx. 85 km² has been covered by lava. The results achieved in this study are in accordance with the reports of the Icelandic Meteorological Office [11], which are based on ground survey and airborne data.

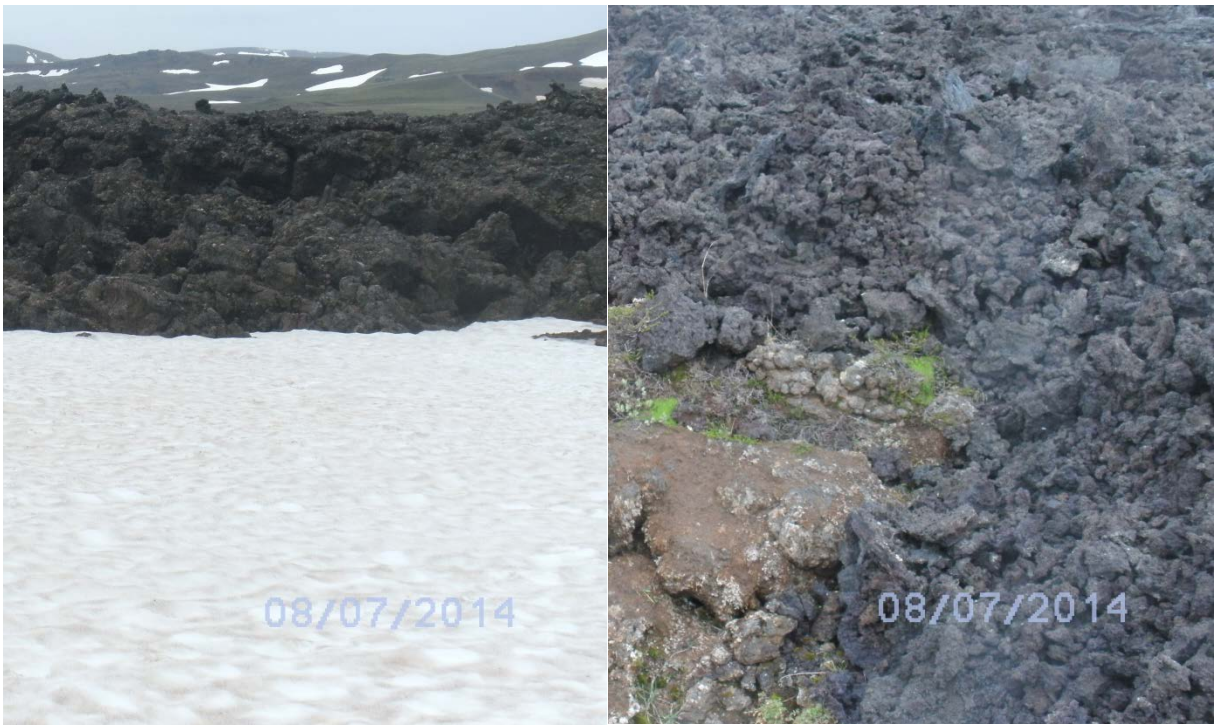

Fig 9: Photographs of the Krafla lava field, which is located ca. 90 km north of the Holuhraun fissure eruption. This lava is the result from eruptions of the Krafla volcano in 1984. Left: Basaltic Aa lava surrounded by snow. Right: Young rough lava surface in the neighborhood to older, more weathered lava. Photographs by the author.

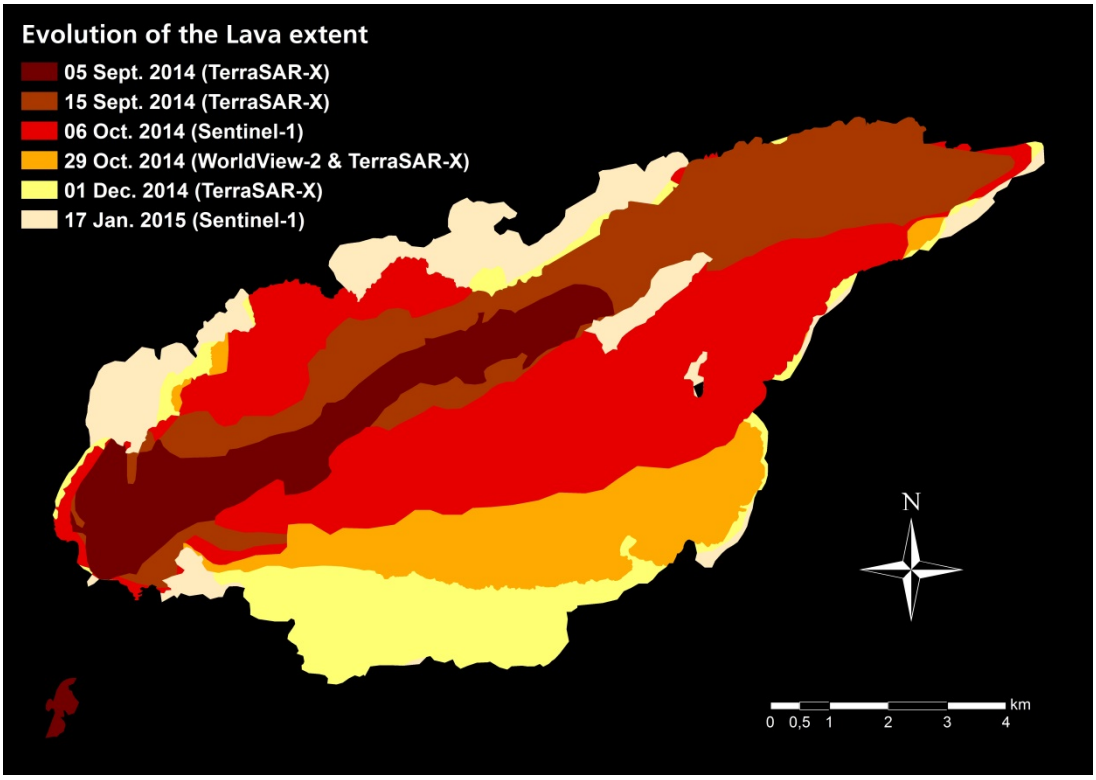

Fig. 10: Spatio-temporal evolution of the lava extent at the Holuhraun fissure eruption, including results of some representative examples of the time series.

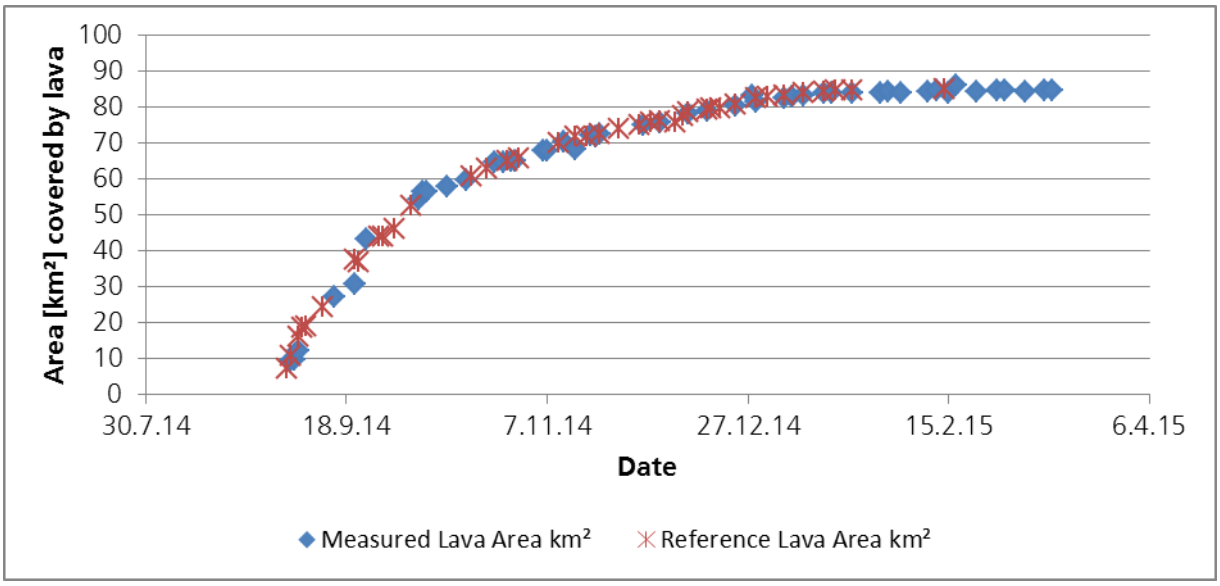

Fig. 11: Spatio-temporal evolution of the lava extent at the Holuhraun fissure eruption. The blue dots show the measurements based on the analysis of satellite data. The red crosses represent reference information from the Icelandic Meteorological Office. The reference information is based on ground survey and airborne data.

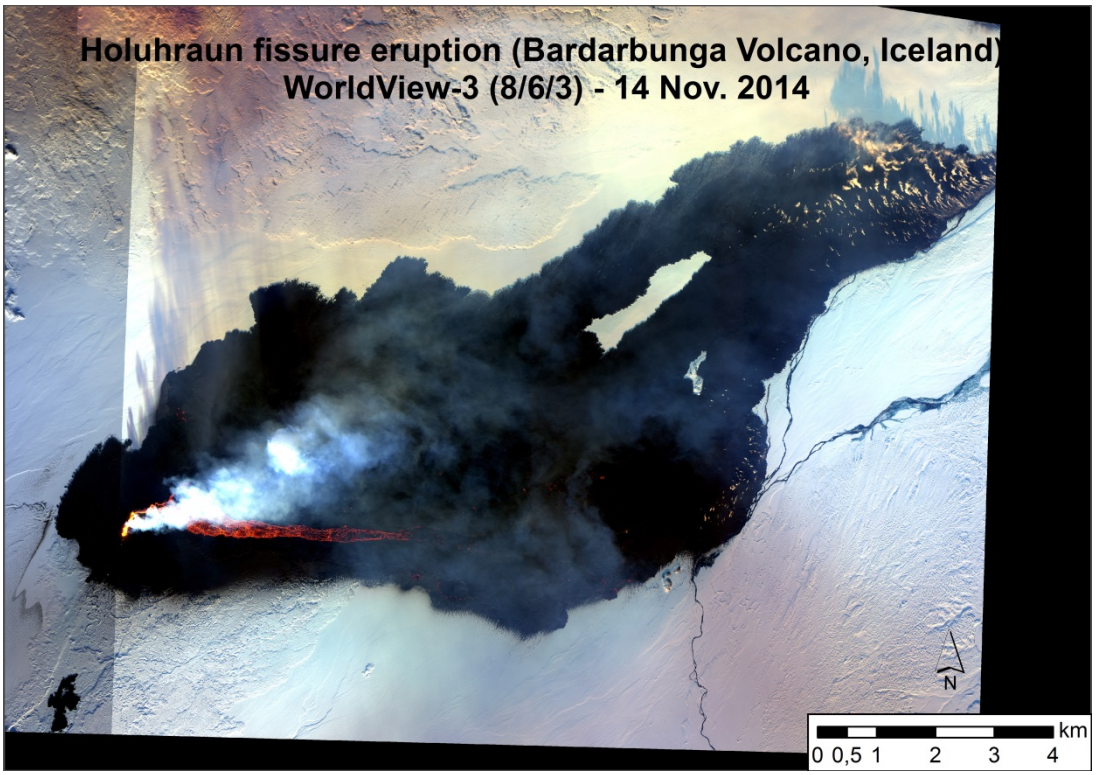

Fig. 12: Very high spatial resolution (0.31 m) WorldView-3 image of the Holuhraun fissure eruption acquired on 14 November 2014. One can clearly differ between the very hot liquid parts of the lava (orange / red) and the lava parts which are already cooled down at the surface (black). The lava field is surrounded by snow. © European Space Imaging/DigitalGlobe.

4. Conclusions

This paper presented a combined analysis of multi-sensor satellite-based remote sensing data monitoring of the 2014/15 Holuhraun fissure eruption in Iceland, one of the largest volcanic events in modern Icelandic history. By the end of the seven months lasting volcanic

eruption, the fissure has extended to a length of over 18 km. An area of approximately 85 km² has been covered by lava.

When comparing the information derived from the SO_2 retrieval (section 3.2) and the spatio-temporal evolution of the lava extent monitored by SAR and optical imagery (section 3.3), the following can be concluded:

We see that (I) the SO_2 signal started to increase when the fissure opened (red line in Fig. 13). (II) The amount of SO_2 increased with increasing lava coverage and length of the fissure. (III) The SO_2 signal decreased to normal (pre-event) level, when the volcanic eruption ended on 28 February 2015 (green line in Fig. 13). The first cloud free imagery of Landsat-8 after the end of eruption, acquired on 02 April 2015, confirms the end of the volcanic activity and shows the final state of the lava extent.

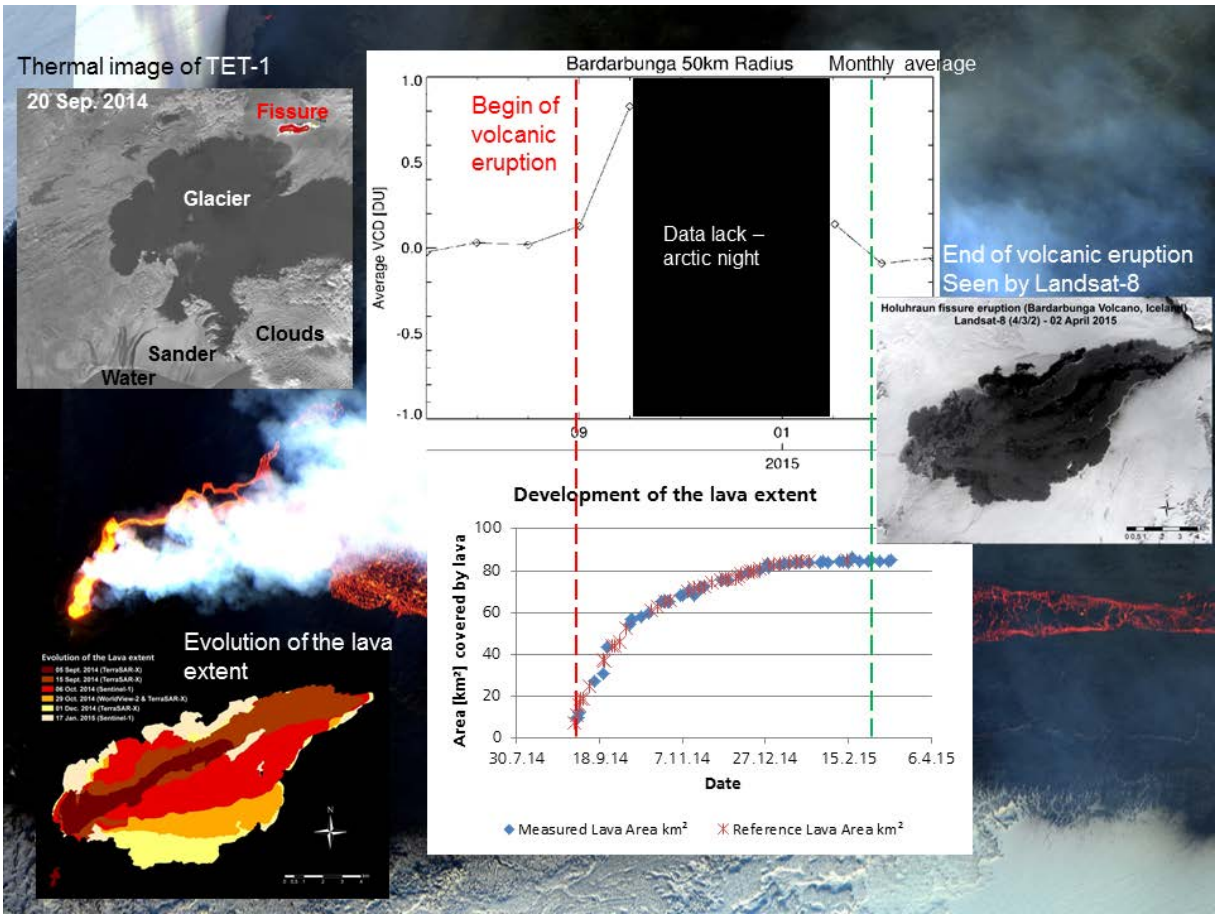

Fig. 13: Comparison of the spatio-temporal evolution of the lava extent and the emission of SO_2. The small image in the right shows the final state of the lava extent (Landsat-8, acquired on 2 April 2015). Background: Detail of the WorldView-3 image of the Holuhraun fissure eruption acquired on 14 November 2014 (© European Space Imaging/DigitalGlobe).

5. Acknowledgements

The author would like to thank Dr. Pascal Hedelt (Remote Sensing Technology Institute, DLR) and Carsten Paproth (Optical Information Systems, DLR) for providing the SO_2 measurements derived from GOME-2 data and the hotspots derived from TET imagery, respectively. The WorldView-2 and -3 imagery were kindly provided by the European Space Imaging Ltd. (EUSI).

6. References

1. Catalogue of Icelandic Volcanoes. http://futurevolc.vedur.is/?volcano=BAR# (last accessed on 01 June 2016).

2. http://volcano.si.edu/volcano.cfm?vn=373030 (last accessed on 01 June 2016).

3. http://earthice.hi.is/bardarbunga_2014#17.08.2014 (last accessed on 01 June 2016).

4. Gudmundsson, A., Lecoeur, N., Mohajeri, N., Thordarson, T. (2014): Dike emplacement at Bardarbunga, Iceland, induces unusual stress changes, caldera deformation, and earthquakes. Bulletin of Volcanology, vol. 76, no. 10, pp. 1-7.

5. Loyola, D., van Geffen, J., Valks, P., Erbertseder, T., Van Roozendael, M., Thomas, W., Zimmer, W., Wißkirchen, K. (2008): Satellite-based detection of volcanic sulphur dioxide from recent eruptions in Central and South America, Advances in Geosciences, vol. 14, 35-40.

6. Rix, M., Valks, P., Hao, N., van Geffen, J., Clerbaux, C., Clarisse, L., Coheur, P.-F., Loyola, D., Erbertseder, T., Zimmer, W., Emmadi, S. (2009): Satellite Monitoring of Volcanic Sulfur Dioxide Emissions for Early Warning of Volcanic Hazards, IEEE Journal of Selected Topics in Applied Earth Observations and Remote Sensing, vol. 2, no. 3, 196-206.

7. Rix, M., Valks, P., Hao, N., Loyola, D., Schlager, H., Huntrieser, H., Flemming, J., Koehler, U., Schumann, U., Inness, A. (2012): Volcanic SO2, BrO and plume height estimations using GOME-2 satellite measurements during the eruption of Eyjafjallajökull in May 2010, Journal of Geophysical Research, vol. 117, D00U19.

8. Thomas, W., Erbertseder, T., Ruppert, T., Van Roozendael, M., Verdebout, J., Balis, D., Meleti, C., Zerefos, C. (2005): On the Retrieval of Volcanic Sulfur Dioxide Emissions from GOME Backscatter Measurements, Journal of Atmospheric Chemistry, vol. 50, 295-320.

9. Torres, R., Snoeij, P., Geudtner, D., Bibby, D., Davidson, M., Attema, E., Potin, P., Rommen, B., Floury, N., Brown, M., Traver, I.N., Deghaye, P., Duesmann, B., Rosich, B., Miranda, N., Bruno, C., L'Abbate, M., Croci, R., Pietropaolo, A., Huchler, M., Rostanet, F. (2012): GMES Sentinel-1 mission. Remote Sensing of Environment 120, 9-24.

10. Lee J.-S., Pottier, E. (2009): Polarimetric Radar Imaging: From Basics to Applications; CRC Press: Boca Raton, FL, USA.

11. Icelandic Meteorological Office: http://en.vedur.is/earthquakes-and-volcanism (last accessed on 01 June 2016).